Progress of Theoretical Physics, Vol. 99, No. 5, May 1998

Evolution of Primordial Protostellar Clouds

—— *Quasi-Static Analysis* ——

Kazuyuki OMUKAI, Ryoichi NISHI, Hideya UEHARA and Hajime SUSA*

Department of Physics, Kyoto University, Kyoto 606-8502, Japan
**Center for Computational Physics, University of Tsukuba*
Tsukuba 305-8577, Japan

(Received February 2, 1998)

The contraction processes of metal-free molecular clouds of starlike mass (or cloud cores) are investigated. We calculate radiative transfer of the H_2 lines and examine quasi-static contraction with radiative cooling. Comparing two time-scales, the free-fall time $t_{\rm ff}$ and the time-scale of quasi-static contraction $t_{\rm qsc}$ ($\sim t_{\rm cool}$, the cooling time) of these cores, we find that the ratio of the two time-scales $t_{\rm ff}/t_{\rm qsc}$, i.e., the efficiency of cooling, becomes larger with contraction even under the existence of cold and opaque envelopes. In particular, for fragments of primordial filamentary clouds, for which $t_{\rm ff} \sim t_{\rm qsc}$ at the fragmentation epoch, they collapse dynamically in the free-fall time-scale. This efficiency of cooling is unique to line cooling.

§1. Introduction

One of the most conspicuous features of galaxies is the existence of stars. To discuss the formation and evolution of galaxies, then, it is indispensable to investigate star formation processes in protogalactic clouds. In addition, stars play crucial roles in galactic activities, for example, ultraviolet radiation and supernova explosions, which are important in some cosmological contexts. Recently, considering the hierarchical clustering scenario, several authors stressed the importance of stars in pregalactic objects for the reionization of the universe (e.g., Ref. 1)). However, the formation of first stars is one of the most poorly understood processes involved in galaxy formation. For this reason, theoretical predictions on the reionization by first stars suffer great uncertainty. Therefore it is definitely well-timed to investigate the formation process of first stars.

The evolution of primordial clouds from which first stars form has been investigated with a one-zone approximation by many authors.[2] However, the mass scale of the clouds which are able to collapse is much larger than the typical stellar mass. Then, we must discuss the fragmentation processes of protogalactic clouds and the evolution of these fragments into stars to understand the star formation.

With respect to the fragmentation process, several authors have envisaged that protogalactic clouds first collapse disk-like, and then fragment into filaments (e.g., Ref. 3)). Uehara et al.[4] investigated the collapse of filamentary primordial clouds with a one-zone approximation and concluded that the minimum mass of the fragments becomes $\sim 1M_\odot$, that is, essentially the Chandrasekhar mass. Their calculation also showed that, for low mass fragments, almost all of hydrogen atoms are converted into molecular form before the fragmentation occurs.

On the other hand, Stahler et al.[5] studied the main accretion phase of a primordial protostar assuming a very low mass hydrostatic core (i.e., a stellar core, see Ref. 6)) initially, and stationary accretion of the envelope onto it. They adopted a higher mass accretion rate ($4.41 \times 10^{-3} M_\odot$ yr^{-1}) than the present-day counterpart ($10^{-5} M_\odot$ yr^{-1}, e.g., Ref. 7)). This higher mass accretion rate is caused by higher temperature $\sim 10^3$ K of primordial gas clouds. However, the question of how a fragment of star-like mass reaches this phase is not considered and still remains unclear. In this paper, we study the evolution of stellar mass primordial clouds shortly after the fragmentation.

How primordial clouds of stellar mass, which are fragments of filamentary clouds, evolve after the fragmentation depends on their efficiency of cooling, i.e., the ratio of the free-fall time-scale $t_{\rm ff}$ to the cooling time-scale $t_{\rm cool}$ (e.g., Ref. 8)). If $t_{\rm ff} < t_{\rm cool}$ (i.e., cooling is not effective), while the cloud cools, it has enough time to adjust itself to a new hydrostatic configuration. Then it contracts, maintaining a nearly hydrostatic equilibrium (i.e., Kelvin-Helmholtz contraction). On the other hand, in the case $t_{\rm ff} > t_{\rm cool}$, the cloud collapses dynamically in its free-fall time-scale after substantial cooling, and no hydrostatic equilibrium is established. In the latter case, the cloud may fragment into smaller pieces again.

At the time of the fragmentation of filamentary clouds, the two time-scales of fragments, $t_{\rm cool}$ and $t_{\rm ff}$, are of the same order of magnitude,[4] since a filamentary cloud fragments when the time-scale of contraction $t_{\rm dyn} \equiv \rho/(d\rho/dt)$ becomes nearly equal to the time-scale of fragmentation $t_{\rm frag} \equiv 2.1/\sqrt{2\pi G\rho}$,[9] where ρ is the density of the cloud. At the epoch of fragmentation, the contraction proceeds isothermally with regard to time. Then $t_{\rm dyn} \simeq (\gamma_{\rm ad} - 1) t_{\rm cool}$, where the adiabatic exponent $\gamma_{\rm ad}$ is 5/3 for monatomic molecules and 7/5 for diatomic molecules. Since the fragmentation time-scale $t_{\rm frag}$ of a filamentary cloud is identical (up to numerical factors) to the free-fall time-scale $t_{\rm ff}$ of a spherical fragment, $t_{\rm cool} \sim t_{\rm ff}$ for the fragment at the fragmentation epoch. Therefore, the nature of the evolution depends on whether the ratio $t_{\rm cool}/t_{\rm ff}$ [more precisely, $t_{\rm qsc}/t_{\rm ff}$, where $t_{\rm qsc}$ is the time-scale of quasi-static contraction (see §3 below)] becomes larger or smaller as a fragment contracts.

To estimate the cooling time, we must investigate the cooling processes in the primordial clouds. The principal difference of a primordial star forming region from its present-day counterpart is its lack of heavy elements and consequently dust grains, which are efficient coolants, keeping present-day molecular clouds almost isothermal (~ 10 K) over many orders of magnitude in density (e.g., Ref. 10)). Therefore, when we investigate primordial star formation, it is no longer possible to impose isothermality. We must study cooling/heating processes and solve the energy equation to determine the temperature. At low temperature ($T < 10^4$ K), the Lyα line of the neutral hydrogen is hardly excited, and there is no atomic cooling process. If there are H_2 molecules, however, these clouds can cool by H_2 rotational/vibrational transition lines. According to Uehara et al.,[4] at the time of fragmentation, filamentary clouds are optically thick for line center frequency of some lines. This should also hold for fragments of them. The surface temperature of the clouds is low, in comparison with the central or averaged temperature. Consequently, the efficiency of cooling by optically thick lines may decrease. For example, the continuum energy

flux decreases as $T_{\rm eff}^4$, where $T_{\rm eff}$ is the effective (photospheric) temperature of a cloud. In an optically thick case, the photosphere is located near the surface, and the low surface temperature causes a severe decrease in the cooling rate. However, in the case that cooling is dominated by optically thick lines, optical depth is not only different from one line to another line, but it also varies with frequency even within one line. In fact, some lines are optically thick at their line center frequencies, but clouds are totally transparent to intervening frequencies between lines. Therefore the notion of a photosphere cannot be easily implemented. Final processed line profiles depend on the structure of the cloud and cannot be known before we calculate radiative transfer resolving frequencies within a single line. Moreover, the number of effective lines changes as the cloud contracts. For these reasons, to understand the evolution of the fragments, it is necessary to treat the H_2 line transfer problem in detail.

The outline of this paper is as follows. In §2, we describe our scheme of the calculation of the luminosity and the cooling rate via the H_2 emission lines for spherical clouds and give some results. In §3, we compare the time-scales $t_{\rm ff}$ and $t_{\rm cool}$ for general initial conditions and discuss the evolution of fragments of filamentary clouds. Some interpretations of the results are also presented in §4. Finally, we summarize our work and discuss its implications with respect to the primordial star formation in §5.

§2. Radiative processes in primordial molecular cloud cores

We consider spherically symmetric gas clouds of starlike mass ($\sim 1M_\odot$) ('molecular cores') composed only of H_2 molecules, because the hydrogen atoms are converted into molecular form before the fragmentation for these low mass fragments.[4] We can neglect helium, since it is thermally inert at these low temperatures. As mentioned above, these clouds lose their thermal energy by radiative cooling via the H_2 rotovibrational lines, and presumably contract into protostars.

In this section, we describe our calculation scheme for the luminosity and cooling rate of a spherically symmetric cloud. The specific intensity I_ν (ergs $\sec^{-1}\mathrm{cm}^{-2}\mathrm{sr}^{-1}$ Hz^{-1}) along a ray is calculated by solving the radiative transfer equation (e.g., Ref. 11)),

$$\frac{dI_\nu}{ds} = -\alpha_\nu I_\nu + j_\nu. \tag{2·1}$$

Here s is the displacement along the ray, and α_ν and j_ν are the absorption and emission coefficients, respectively. These coefficients can be written by using Einstein A- and B- coefficients:

$$j_\nu = \frac{h\nu}{4\pi} n_2 A_{21} \phi(\nu), \tag{2·2}$$

$$\alpha_\nu = \frac{h\nu}{4\pi} \phi(\nu)(n_1 B_{12} - n_2 B_{21}). \tag{2·3}$$

Here n_1 and n_2 are the number densities of the molecules in the lower and upper level of the transition, respectively, and $\phi(\nu)$ is the line profile function. In our

calculation, the line center optical depth of the lines across a cloud τ_c is no more than several hundreds. Since Lorentz wings of a line become more important than its Doppler core only when τ_c is as large as 10^3, we only consider line broadening owing to the thermal Doppler effect, i.e.,

$$\phi(\nu) = \frac{1}{\Delta\nu_D\sqrt{\pi}} e^{-(\nu-\nu_0)^2/(\Delta\nu_D)^2}. \tag{2·4}$$

Here ν_0 is the line center frequency, and the Doppler width $\Delta\nu_D$ is defined by

$$\Delta\nu_D = \frac{\nu_0}{c}\sqrt{\frac{2kT}{\mu m_H}}, \tag{2·5}$$

where T is the temperature at each radius in the cloud, $m_H = 1.67 \times 10^{-24}$ g is the mass of a hydrogen atom, and $\mu = 2$ is the molecular weight of the molecular hydrogen. We include the first three vibrational states, with rotational levels up to $j = 20$ in each state, following Palla et al.[2] We take A-coefficients of molecular hydrogen from Turner et al.[12] B-coefficients can be obtained from A-coefficients by the following Einstein relations,

$$g_1 B_{12} = g_2 B_{21}, \tag{2·6}$$

$$A_{21} = \frac{2h\nu_0^3}{c^2} B_{21}, \tag{2·7}$$

where g_i is the statistical weight of the level i. The critical number density n_{cr}, where radiative and collisional deexicitation rates become equal for molecular hydrogen, is $\sim 10^4$ cm^{-3}. For a typical number density of fragments ($\sim 10^{10}$ cm$^{-3} \gg n_{cr}$), almost all excited molecules would be deexcited by collision with other molecules. Therefore, collisional local thermodynamic equilibrium (LTE) is established, and scattering of photons can be neglected. These properties make the transfer problem of H_2 lines fairly tractable.

Figure 1 displays the geometry of grids of the radiative transfer calculation in the case of spherical symmetry (Ref. 13); see also Ref. 14)). To know the luminosity at the i-th radial grid r_i, we solve the transfer equation (2·1) with frequency ν along

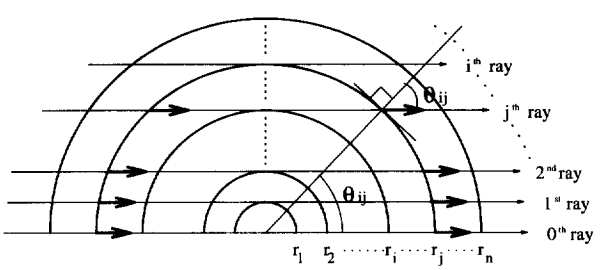

Fig. 1. Ray geometry of radiative transfer calculation in spherical symmetry. We solve frequency-by-frequency radiative transfer equations along rays tangent to each mass shell and obtain the intensity $I_\nu(\theta)$ at each mesh point.

from the 0-th to $(i-1)$-th rays, and we obtain the specific intensity at r_i in the direction θ_{ij}, $I_\nu(r_i, \theta_{ij})$ $(-i+1 \leq j \leq i-1)$. This procedure will be repeated for each frequency mesh. We consider the frequency range for each line within four times the Doppler width corresponding to the central temperature from the line center. Each line is usually separated into 20 frequency meshes (in some cases, e.g., Fig. 7, 80 frequency meshes), and the number of radial meshes n is 50 in our runs. Integrating over θ and ν, we obtain the monochromatic energy flux F_ν and the luminosity L:

$$F_\nu(r) = 2\pi \int_0^\pi I_\nu(r, \theta) \cos\theta d\theta, \tag{2·8}$$

$$L(r) = 4\pi r^2 \int_0^\infty F_\nu(r) d\nu. \tag{2·9}$$

As for cooling rate per unit mass $\Lambda(m)$, we differentiate the luminosity L with respect to the Lagrangian mass coordinate m,

$$\Lambda(m) = \frac{\partial L}{\partial m}, \tag{2·10}$$

$$m(r) = \int_0^r 4\pi r'^2 \rho dr'. \tag{2·11}$$

Figure 2 displays the contribution from each line to the luminosity at the surface of a typical cloud. The mass of the cloud is $1M_\odot$, the number density at half mass radius is 10^{11} cm^{-3}, and the density/temperature distribution is represented by the Emden function of polytropic index 2.5. In this spectrum, there is a gap around the wavelength of 4μm, and lines can be classified into longer and shorter wavelength groups. The shorter and longer wavelength lines correspond to transitions with and without changes of vibrational levels.

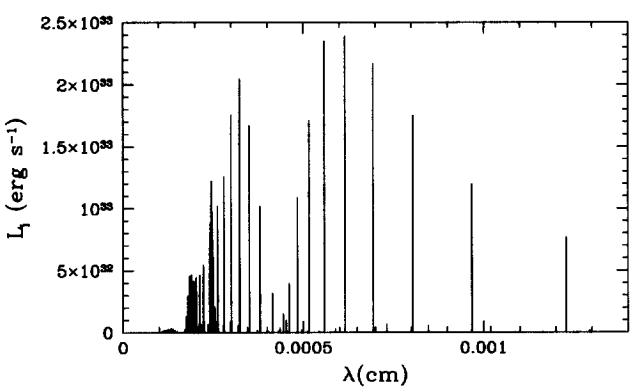

Fig. 2. The contribution from each line to the luminosity at the surface versus its wavelength. The mass of the cloud is $1M_\odot$, the number density at half mass radius is 10^{11} cm^{-3}, and the density/temperature distribution is represented by the Emden function of polytropic index 2.5.

§3. Evolution of fragments

As initial conditions, we assume polytropic gas spheres in hydrostatic equilibrium; namely the density/temperature distribution is represented by the Emden function of polytropic index N. Clouds are cut off at the radius r_s, where the density falls off by a factor of 10^{-3} from the central value. Therefore, parameters characterizing initial conditions are the effective polytropic index N, the total mass of the cloud M, and the number density n_h at the half mass radius. For a given initial configuration, we can obtain the specific entropy distribution $s(m, t = 0)$.

We then bring forward the cloud one time step Δt *quasi-statically* in the following way. We calculate the cooling rate $\Lambda(m)$ as described in §2, and advance the specific entropy distribution $s(m, t)$ by one time step Δt using the heat equation

$$\frac{\partial s}{\partial t} = -\frac{1}{T}\Lambda(m). \tag{3·1}$$

With the entropy distribution at the next time step $s(m, t + \Delta t) = s(m, t) - (\Lambda(m)/T)\Delta t$, we find the new equilibrium configuration using the equations of hydrostatic equilibrium,

$$\frac{\partial r}{\partial m} = \frac{1}{4\pi r^2 \rho}, \tag{3·2}$$

$$\frac{\partial p}{\partial m} = -\frac{Gm}{4\pi r^4}, \tag{3·3}$$

and the equation of state,

$$p \propto \exp[s/c_{\rm v}]\rho^{\gamma_{\rm ad}}. \tag{3·4}$$

Here $\gamma_{\rm ad} = 7/5$ is the adiabatic coefficient and $c_{\rm v} = \frac{1}{\gamma_{\rm ad}-1}\frac{k}{\mu m_{\rm H}}$ is specific heat of hydrogen molecule at constant volume. We impose a constant external pressure at the outer boundary. For dense and cold clouds, like the fragments under consideration, radiation pressure can be neglected, and the pressure can be assumed to be given by the gas pressure only.

For given states of clouds, we compare two time-scales, i.e., the free-fall time

$$t_{\rm ff}(m) \equiv \sqrt{\frac{3\pi}{32G\bar{\rho}(m)}}, \tag{3·5}$$

and the time-scale of quasi-static contraction,

$$t_{\rm qsc}(m) \equiv \rho / \left(\frac{\partial \rho}{\partial t}\right)_{m,\text{quasi-static}}. \tag{3·6}$$

Here, $\bar{\rho}(m)$ is the mean density within the mass coordinate m, and each quantity is evaluated at the coordinate m. From the virial theorem, $t_{\rm qsc}$ is of the same order of magnitude of $t_{\rm cool}$.

Figure 3 shows the contours of the ratio $t_{\rm ff}/t_{\rm qsc}$ at the center ($m = 0$) of clouds with (a) $N = 2.5$ (adiabatic stratification) and (b) $N = 8$. Regions around the

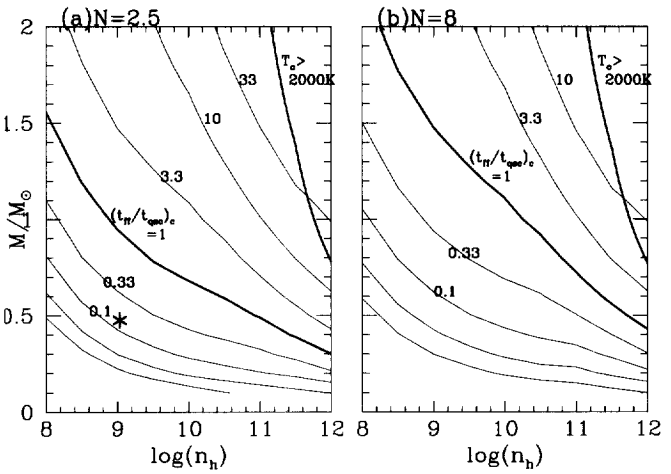

Fig. 3. Contours of the ratio $t_{\rm ff}/t_{\rm qsc}$ at the center of clouds of polytropic index (a) $N = 2.5$ and (b) $N = 8$. The contour spacing is logarithmic with an increment of 0.5. The upper-right regions correspond to the temperature $T > 2000$ K, where hydrogen molecules begin to dissociate.

curves $t_{\rm ff}/t_{\rm qsc} = 1$ are expected to be initial states of fragments. Although Fig. 3 displays the values at the center, this ratio does not change significantly within a cloud, except near the surface. The upper-right regions correspond to higher central temperature > 2000 K, where the molecular hydrogen begins to dissociate. From the two panels of Fig. 3, we can see that the ratio $t_{\rm ff}/t_{\rm qsc}$ depends only slightly on the effective polytropic indices N, rather than on masses and densities. Note that for clouds of the same mass, the ratio $t_{\rm ff}/t_{\rm qsc}$ is greater for denser cloud. This implies that as a cloud contracts, the ratio $t_{\rm ff}/t_{\rm qsc}$ becomes larger. In particular, for fragments of filamentary gas clouds, for which $t_{\rm ff} \sim t_{\rm qsc}$ initially, $t_{\rm qsc}$ becomes shorter than $t_{\rm ff}$ as they contract; i.e., such clouds collapse dynamically. Note that when $t_{\rm qsc} < t_{\rm ff}$, clouds do not contract quasi-statically, and $t_{\rm qsc}$ does not possess the meaning of the collapse time-scale. In this case, $t_{\rm qsc}$ merely measures the time-scale of cooling.

The discussion above is for fixed N. However, these clouds change their entropy distribution as they contract. Therefore it is not enough to discuss their evolution only with fixed N. We need to calculate the evolution of clouds contracting quasi-statically and to show that they in fact begin to collapse dynamically. We choose initial conditions under which clouds contract quasi-statically and pursue their evolution. Their initial parameters are (a) $M = 0.5M_\odot$, $n_h = 10^9$ cm^{-3}, $N = 2.5$ (the asterisk $*$ in Fig. 3(a)), and (b) $M = 0.2M_\odot$, $n_h = 10^9$ cm^{-3}, $N = 20$. For the parameter representing the structure of clouds, we employ the effective exponents for structure,

$$\gamma_{\rm str}(m) \equiv \frac{(\partial \ln p/\partial m)_t}{(\partial \ln \rho/\partial m)_t}. \tag{3·7}$$

Figure 4 displays changes of the $\gamma_{\rm str}(m)$ as the clouds contract. We can see

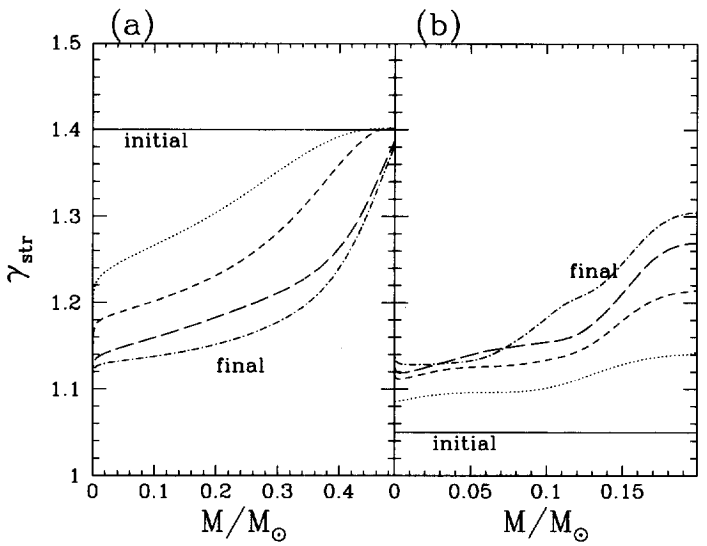

Fig. 4. Evolution of the effective exponent for structure, $\gamma_{str}(m) \equiv \frac{(\partial \ln p/\partial m)_t}{(\partial \ln \rho/\partial m)_t}$, for two quasi-statically contracting clouds. The initial conditions (solid lines) are (a) $M = 0.5M_\odot$, $n_h = 10^9$ cm^{-3}, $N = 2.5$. (b) $M = 0.2M_\odot$, $n_h = 10^9$ cm^{-3}, $N = 20$. Each curve depicts $\gamma_{str}(m)$ at some specific time (in order of time: solid, dotted, short-dashed, long-dashed and dash-dotted line). The central temperature and density are (a) initial: 149 K, 1.35×10^{-14} gcm^{-3}, final: 2048 K, 1.50×10^{-10} gcm^{-3} and (b) initial: 89 K, 2.48×10^{-14} gcm^{-3}, final: 2154 K, 4.41×10^{-9} gcm^{-3}. These values approach $1.12-1.13$ around the central region for both clouds when the central temperature reaches $\sim$ 2000 K. Note that both clouds start to dynamical collapse before reaching the final states shown in the figure. Therefore, our quasi-static formulation cannot be applied, and thereafter the evolution shown in the figure does not correspond to the actual evolution of the clouds.

that values of $\gamma_{str}(m)$ become nearly flat and approach $1.12 - 1.13$ when the central temperature reaches $\sim$ 2000 K, which is the dissociation temperature of H_2. These values of γ_{str} correspond to $N \simeq 8$, regardless of the initial N values. However, for the fragments, the clouds start to collapse dynamically before these states are reached. In such a case, this limiting value of N has no significant meaning. But the very existence of the limiting value supports our discussion above with fixed N. In fact, from Fig. 5, where the change of time-scales and their ratio are shown for the case (a) of Fig. 4, we can see that the cloud indeed collapses dynamically after it contracts quasi-statically to some extent.

Although γ_{str} becomes $\simeq 1.13$, the effective exponent for temporal evolution of a fixed mass element,

$$\gamma_{ev}(m) \equiv \frac{(\partial \ln p/\partial t)_m}{(\partial \ln \rho/\partial t)_m}, \tag{3·8}$$

has different value. The distributions of γ_{ev} at different times are shown in Fig. 6. Effective adiabatic coefficients, γ_{ev}, are always nearly equal to 4/3 in the case of quasi-static contraction. The reason for this is that the relation between γ_{ev} and

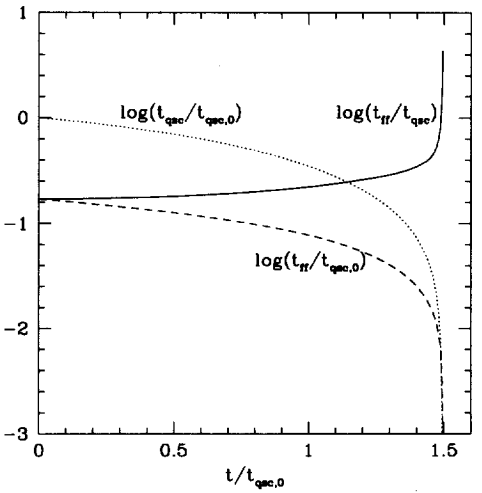

Fig. 5. Evolution of free-fall time $t_{\rm ff}$ and dynamical time for quasi-static contraction $t_{\rm qsc}$ at the center and their ratio for a cloud which contracts quasi-statically at the beginning (case (a) of Fig. 4). The time-scales $t_{\rm ff}$ and $t_{\rm qsc}$ and the time elapsed from the beginning t are all normalized by $t_{\rm qsc,0}$, the initial value of $t_{\rm qsc}$. This figure indeed shows the cloud begins to collapse dynamically after $\sim 1.5 t_{\rm qsc,0}$.

$\gamma_{\rm ad}$ $(= 7/5)$ is

$$\gamma_{\rm ev} = \gamma_{\rm ad} - \frac{t_{\rm qsc}}{t_{\rm cool}}, \tag{3·9}$$

where $t_{\rm cool} = \varepsilon/(\partial L/\partial m)$ and $\varepsilon(\equiv \frac{1}{\gamma_{\rm ad}-1}\frac{kT}{\mu m_{\rm H}})$ is internal energy per unit mass. From the virial theorem,

$$3(\gamma_{\rm ad} - 1)E_{\rm i} + E_{\rm g} = 0, \tag{3·10}$$

we find that

$$\left|E_{\rm i}/\frac{dE_{\rm i}}{dt}\right| = \left|E_{\rm g}/\frac{dE_{\rm g}}{dt}\right|, \tag{3·11}$$

where $E_{\rm i}$ and $E_{\rm g}$ are the total internal energy and gravitational energy:

$$E_{\rm i} = \int_0^M \varepsilon dm, \quad E_{\rm g} = -\int_0^M \frac{Gm}{r} dm. \tag{3·12}$$

In the case of homologous contraction, $E_{\rm g} \propto \rho^{1/3}$, where we compare ρ for a fixed mass element (a homologous point), and $t_{\rm qsc}$ becomes constant along the radial coordinate:

$$t_{\rm qsc} = \left(\rho/\frac{d\rho}{dt}\right) = \frac{1}{3}\left|E_{\rm g}/\frac{dE_{\rm g}}{dt}\right|. \tag{3·13}$$

On the other hand, by using total energy of a cloud,

$$W = E_{\rm i} + E_{\rm g} = 3\left(\frac{4}{3} - \gamma_{\rm ad}\right)E_{\rm i}, \tag{3·14}$$

its total luminosity can be given as

$$L = \frac{dW}{dt} = 3\left(\gamma_{\rm ad} - \frac{4}{3}\right)\left|\frac{dE_{\rm i}}{dt}\right|. \tag{3·15}$$

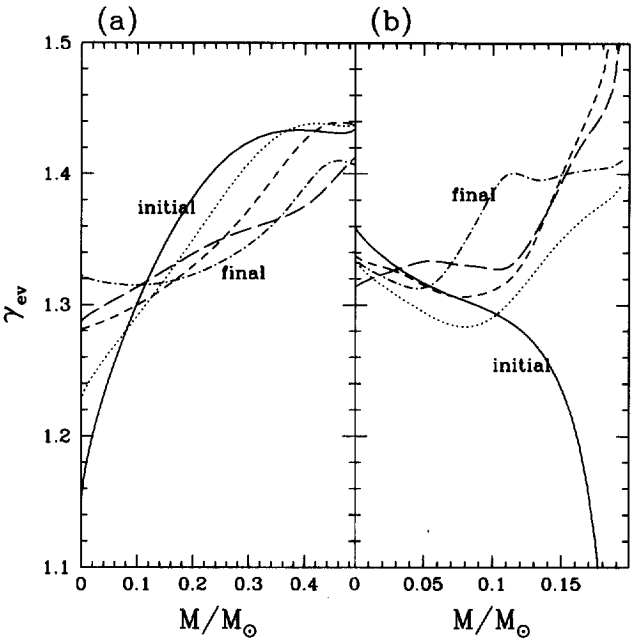

Fig. 6. Evolution of the effective exponent for temporal evolution, $\gamma_{ev}(m) \equiv \frac{(\partial \ln p/\partial t)_m}{(\partial \ln \rho/\partial t)_m}$, for the same clouds as in Fig. 4. Here the same line corresponds to the same time as in Fig. 4.

The mean cooling time-scale becomes

$$\langle t_{\rm cool} \rangle = \frac{E_{\rm i}}{L} = \frac{1}{3\left(\gamma_{\rm ad} - \frac{4}{3}\right)} \left| E_{\rm i} / \frac{dE_{\rm i}}{dt} \right| . \tag{3·16}$$

Therefore, for homologously contracting spherical clouds, we have

$$t_{\rm qsc} = \left(\gamma_{\rm ad} - \frac{4}{3}\right) \langle t_{\rm cool} \rangle . \tag{3·17}$$

For the case of non-homogeneous contraction, this equation is not exactly valid. However, holds approximately in this case. From Eq. (3·9), (3·17) and identifying global cooling time-scale $\langle t_{\rm cool} \rangle$ with local one $t_{\rm cool}$, $\gamma_{\rm ev}$ becomes nearly equal to $\frac{4}{3}$ as a whole. From Fig. 6, it can be seen that the initial steep gradients of the $\gamma_{\rm ev}$ are levelled, and they assume values around 4/3. This is because there exists a limiting structure for clouds contracting quasi-statically, and then the contraction becomes roughly homologous.

§4. Interpretation of results

In §3 above, we have shown that the stellar mass molecular cores collapse dynamically, although some lines are optically thick at line center. This fact indicates that the efficiency of cooling by H_2 lines does not fall significantly even in such a situation, in contrast to the case of continuous radiation. The reason for this can be interpreted as follows.

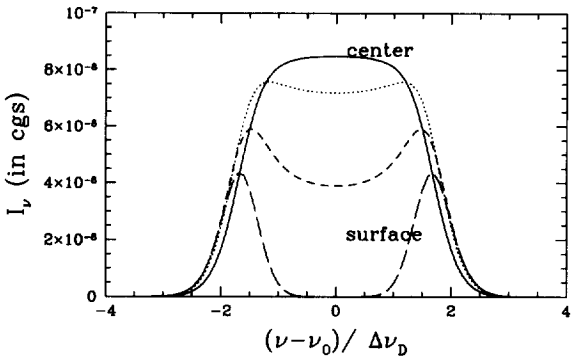

Fig. 7. Processed line profiles of an optically thick line along a ray passing through the center of the cloud at the radii containing 0 % (center, solid line), 1.4 % (dotted line), 9.9 % (short dashed line), and 100 % (surface, long dashed line) of the total mass. The optical depth at the line-center frequency τ_c = 38, 46, 54 and 76, respectively, measured from the surface of incidence. The line corresponds to the transition from (v = 1, j = 3) to (v = 0, j = 1). The parameters of the cloud are the same as in Fig. 2. The abscissa represents frequency from line center normalized by the Doppler width at the center of the cloud $\Delta\nu_{D,c}$.

Figure 7 displays the change of a processed profile of a single optically thick line (optical depth at line center across the cloud is 76) along a ray passing through the center of the cloud. Since the cloud is optically thick at line center, the specific intensity at line center is saturated with the blackbody value determined from the local temperature. On the other hand, optical depth at wing is smaller than unity. The final processed profile at the cloud surface is double peaked, and the peak frequencies correspond to frequencies where the optical depth across the core $\tau_{\nu,\mathrm{core}} > 1$ (i.e., the radiation is saturated with the value of the core temperature) and that of envelope $\tau_{\nu,\mathrm{env}} < 1$ (i.e., the radiation can be larger than the value of the envelope temperature). The height (i.e., the normalization of intensity) and width of these peaks are of the same order of magnitude as the blackbody value determined from the temperature near the center, not around the surface of the cloud. The reduction factors from the central values are only several. Owing to the effect described above, which is a distinctive feature of line cooling, the temperature around the cloud center can be 'seen' from outside the cloud, even when lines are optically thick at line center and the surface temperature is relatively low. Accordingly, its cooling proceeds efficiently, as long as there are enough frequency ranges where $\tau_{\nu,\mathrm{core}} > 1$ and $\tau_{\nu,\mathrm{env}} < 1$. Therefore, the decrease in the efficiency of cooling caused by the low surface temperature is not severe in the line cooling case, in contrast to the case of cooling by continuum.

Figure 8 displays the ratio of L_i, the contribution to the luminosity at the surface from each line i, to $L_{\mathrm{thin},i}$, the value in the "optically thin" case (i.e., $L(r_s) = \sum_{i=\mathrm{all\ lines}} L_i$, and $L_{\mathrm{thin},i} = 4\pi \int_{\mathrm{whole\ cloud}} dV \int_{\mathrm{line}\ i} d\nu j_\nu$), versus optical depths at line center across the clouds $\tau_{\mathrm{c,tot}}$ for each line. All marks of a given variety represent lines of a single given cloud, and the solid curve represents the value of $L_i/L_{\mathrm{thin},i}$ for the uniform cloud of $1M_\odot$, whose number density equals 10^{11} cm^{-3}. From this

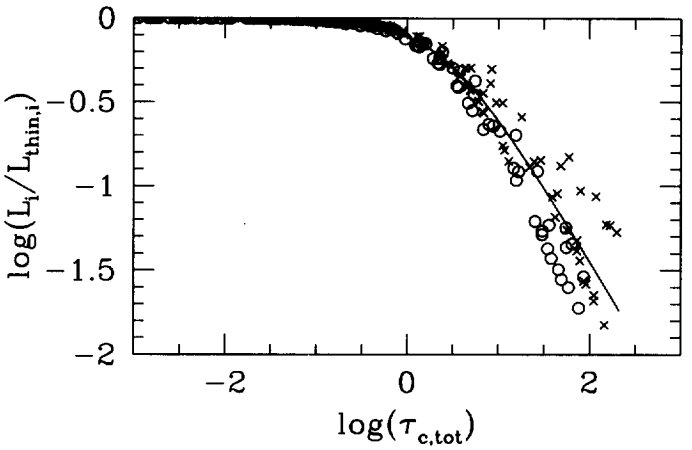

Fig. 8. The ratio of L_i, the contribution to the luminosity at the surface from each line i, to $L_{\mathrm{thin},i}$, the value in the "optically thin" case, as a function of the optical depth at line-center frequency across the clouds $\tau_{\mathrm{c,tot}}$ for each line. These relations are demonstrated for two clouds. Open circles and crosses correspond to lines from the cloud of ($N = 2.5$, $M = 1M_\odot$, $n_h = 10^{11}$ cm^{-3}) and ($N = 8$, $M = 1M_\odot$, $n_h = 10^{11}$ cm^{-3}), respectively. The solid curve represents $L_i/L_{\mathrm{thin},i}$ for uniform clouds.

figure, it can be seen that $L_i/L_{\mathrm{thin},i}$ falls only as $\sim {\tau_{\mathrm{tot}}}^{-1}$. This simply reflects the fact that in the "optically thin" case, the specific intensity along a ray at optical depth τ (even if $\tau > 1$) is determined as

$$I_{\nu,\mathrm{thin}} = \int_0^\tau S_\nu(\tau')d\tau', \tag{4·1}$$

where $S_\nu = j_\nu/\alpha_\nu$ is the source function. On the other hand, in the optically thick case,

$$I_\nu \sim S_\nu(\tau). \tag{4·2}$$

Then, if $\tau > 1$

$$I_\nu/I_{\nu,\mathrm{thin}} \sim \tau^{-1}. \tag{4·3}$$

Therefore, no significant suppression of cooling caused by the low surface temperature arises in Fig. 8.

As discussed above, the effects of the surface temperature are not severe even for optically thick lines. Thus it is appropriate to use the value of a homogeneous cloud in estimating the cooling time. This is given by

$$t_{\mathrm{cool}} = \frac{E_{\mathrm{i}}}{L} = \frac{Mc_{\mathrm{v}}T}{4\pi R^2\sigma T^4 f} \propto M^{1/3}T^{-3}n^{2/3}f^{-1}, \tag{4·4}$$

where $E_{\mathrm{i}}, M, T, R, c_{\mathrm{v}}$ and n are the internal energy, the mass, the temperature, the radius, the specific heat at constant volume, and the number density of the homogeneous cloud, respectively. The quantity f is the ratio of the luminosity of the cloud to the blackbody luminosity of the temperature T. In the case that cooling is dominated by line cooling, by using the line width $\Delta\nu$ and the effective number

of lines α_c, f can be written as $f = L/4\pi R^2\sigma T^4 \sim \alpha_c \frac{\Delta\nu}{\nu}$. We adopt the Doppler width $\frac{\Delta\nu_D}{\nu} = \frac{1}{c}\sqrt{\frac{2kT}{\mu m_H}}$ for the line width. Assuming the cloud is almost in hydrostatic equilibrium initially, we can relate the temperature with the mass and the number density: $T \propto M^{2/3}n^{1/3}$. From these relations, we obtain

$$t_{cool} \propto M^{-2}n^{-1/2}\alpha_c^{-1}. \tag{4·5}$$

On the other hand, the free-fall time is given by

$$t_{ff} = \sqrt{\frac{3\pi}{32G\rho}} \propto n^{-1/2}. \tag{4·6}$$

Then the ratio of these two time-scales is

$$\frac{t_{ff}}{t_{cool}} \propto M^2\alpha_c. \tag{4·7}$$

As the cloud contracts, the number of optically thick lines (in this case, α_c) increases, and the ratio t_{ff}/t_{cool} becomes larger. This accounts for the results of numerical calculation described above (see also Ref. 4) and 15)).

§5. Conclusion and discussion

Our principal result is that if cooling is dominated by H_2 line cooling, a primordial cloud of stellar mass scale is able to cool efficiently. This is because the efficiency of line cooling does not decrease significantly by the effect of a line profile, even when the cloud is optically thick for line center frequency and its surface temperature is relatively low. In particular, fragments of filamentary clouds collapse dynamically after fragmentation. Although our calculation is limited to $\sim 1M_\odot$ composed only of H_2, our results can be applied to more general molecular cores, as long as cooling is dominated by optically thick line emissions.

A dynamically collapsing spherical gas cloud is unstable to a non-spherical perturbation and becomes disk-like.[16] Therefore, dynamically collapsing fragments may also become disk-like. Since a self-gravitating disk is unstable to fragmentation, cloud cores may fragment again. Whether repeated fragmentations are possible or not depends on the thickness of the disk. Fragmentation occurs for a thin disk (axis ratio $> 2\pi$), but does not occur for a thick disk.[17] Because fragments of filamentary clouds start collapsing from nearly hydrostatic equilibrium, it seems unlikely that they reach a highly flattened configuration. Therefore it is expected that even if fragmentation were to occur, it would not be the case that numerous small pieces would be produced.

Uehara et al.[4] investigated the fragmentation of filamentary clouds with a one-zone approximation. Recently, Nakamura and Umemura[18] examined cylindrical collapse of primordial clouds with radial structures and showed that at the epoch of fragmentation the clouds display clear core-envelope structures. They suggested that Uehara et al.'s[4] one-zone clouds correspond to the cores of their clouds. Hence, if the contraction of fragments were slow, the cores would accrete ambient gas. This

would result in more massive ones. However, our analysis shows the contraction is sufficiently rapid (its time-scale is the free-fall time-scale in the core). Thus the accretion of the envelope (its time-scale is the free-fall time-scale in the envelope), if it exists, becomes significant only after the molecular core contracts sufficiently into a stellar core. The accretion of the envelope does not affect the dynamics of the contracting core significantly. Consequently, it is possible to treat the contraction of the core and the accretion of ambient gas separately.

In this work, we showed that fragments of filamentary clouds collapse dynamically, although we have not pursued yet the actual evolution of the cloud after they begin dynamical collapse. To elucidate the actual contraction of primordial protostellar clouds, elaborate hydrodynamical calculations are needed. This will be presented in a forthcoming paper.[19]

Acknowledgements

We would like to thank Professor H. Sato for continuous encouragement and Professor N. Sugiyama for critical reading of the manuscript. This work is supported in part by Research Fellowships of the Japan Society for the Promotion of Science for Young Scientists, No.6894 (HU), 2370 (HS) and by the Grant-in-Aid for Scientific Research from the Ministry of Education, Science, Sports and Culture No. 09740174 (RN).

References

1) M. Fukugita and M. Kawasaki, Mon. Not. R. Astron. Soc. **269** (1994), 563.
J. P. Ostriker and N. Y. Gnedin, Astrophys. J. **472** (1996), L63.
Z. Haiman and A. Loeb, Astrophys. J. **483** (1997), 21.
2) T. Matsuda, H. Sato and H. Takeda, Prog. Theor. Phys. **42** (1969), 219.
T. Yoneyama, Publ. Astron. Soc. Jpn. **24** (1972), 87.
J. B. Hatchins, Astrophys. J. **205** (1976), 103.
Y. Yoshii and Y. Sabano, Publ. Astron. Soc. Jpn. **31** (1979), 305.
R. G. Carlberg, Mon. Not. R. Astron. Soc. **197** (1981), 1021.
F. Palla, E. E. Salpeter and S. W. Stahler, Astrophys. J. **271** (1983), 632.
J. Silk, Mon. Not. R. Astron. Soc. **205** (1983), 705.
Yu. I. Izotov and I. G. Kolesnik, Soviet Astro. **28** (1984), 15.
O. Lahav, Mon. Not. R. Astron. Soc. **220** (1986), 259.
D. Puy and M. Signore, Astron. Astrophys. **305** (1996), 371.
D. Puy and M. Signore, New Astronomy **2** (1997), 299.
3) H. Susa, H. Uehara and R. Nishi, Prog. Theor. Phys. **96** (1996), 1073.
4) H. Uehara, H. Susa, R. Nishi, M. Yamada and T. Nakamura, Astrophys. J. **473** (1996), L95.
5) S. W. Stahler, F. Palla and E. E. Salpeter, Astrophys. J. **302** (1986), 590.
6) R. B. Larson, Mon. Not. R. Astron. Soc. **145** (1969), 271.
7) S. W. Stahler, F. H. Shu and R. E. Taam, Astrophys. J. **241** (1980), 637.
8) M. J. Rees and J. P. Ostriker, Mon. Not. R. Astron. Soc. **179** (1977), 541.
9) M. Nagasawa, Prog. Theor. Phys. **77** (1987), 635.
10) C. Hayashi and T. Nakano, Prog. Theor. Phys. **34** (1965), 754.
T. Hattori, T. Nakano and C. Hayashi, Prog. Theor. Phys. **42** (1969), 781.
11) G. B. Rybicki and A. P. Lightman, *Radiative Processes in Astrophysics* (Wiley-Interscience, New York, 1979), Chap. 1.
12) J. Turner, K. Kirby-Docken and A. Dalgarno, Astrophys. J. Supplement **35** (1977), 281.
13) D. H. Hummer and G. B. Rybicki, Mon. Not. R. Astron. Soc. **152** (1971), 1.

14) H. Masunaga, S. M. Miyama and S. Inutsuka, Astrophys. J. **495** (1998), 346.
15) C. Low and D. Lynden-Bell, Mon. Not. R. Astron. Soc. **176** (1976), 367.
M. J. Rees, Mon. Not. R. Astron. Soc. **176** (1976), 483.
J. Silk, Astrophys. J. **214** (1977), 152.
16) C. C. Lin, L. Mestel and F. H. Shu, Astrophys. J. **142** (1965), 1431.
17) P. Goldreich and D. Lynden-Bell, Mon. Not. R. Astron. Soc. **130** (1965), 97.
18) F. Nakamura and M. Umemura, private communication.
19) K. Omukai and R. Nishi, Astrophys. J., submitted.